Lagrangian statistics of particle pairs in homogeneous isotropic turbulence

L. Biferale
Dipartimento di Fisica, Università "Tor Vergata," and INFN, Sezione di Roma II,
Via della Ricerca Scientifica 1, I-00133 Roma, Italy

G. Boffetta
Dipartimento di Fisica Generale and INFN, Università di Torino, Via P.Giuria 1, I-10125 Torino, Italy

A. Celani
CNRS, INLN, 1361 Route des Lucioles, F-06560 Valbonne, France

B. J. Devenish
Dipartimento di Fisica, Università "Tor Vergata," and INFN, Sezione di Roma II,
Via della Ricerca Scientifica 1, I-00133 Roma, Italy and The Met Office, Fitzroy Road, Exeter,
Devon EX1 3PB, United Kingdom

A. Lanotte[a]
CNR, ISAC, Str. Prov. Lecce-Monteroni km 1.2, I-73100 Lecce, Italy

F. Toschi
CNR, IAC, Viale del Policlinico 137, I-00161 Roma, Italy
and INFN, Sezione di Ferrara, Via G. Saragat 1, I-44100 Ferrara, Italy

We present a detailed investigation of the particle pair separation process in homogeneous isotropic turbulence. We use data from direct numerical simulations up to $R_\lambda \sim 280$ following the evolution of about two million passive tracers advected by the flow over a time span of about three decades. We present data for both the separation distance and the relative velocity statistics. Statistics are measured along the particle pair trajectories both as a function of time and as a function of their separation, i.e., at fixed scales. We compare and contrast both sets of statistics in order to gain insight into the mechanisms governing the separation process. We find very high levels of intermittency in the early stages, that is, for travel times up to order ten Kolmogorov time scales. The fixed scale statistics allow us to quantify anomalous corrections to Richardson diffusion in the inertial range of scales for those pairs that separate rapidly. It also allows a quantitative analysis of intermittency corrections for the relative velocity statistics. © *2005 American Institute of Physics.*
[DOI: 10.1063/1.2130742]

I. INTRODUCTION

The relative dispersion of pairs of particles is important because of its connection with the problem of concentration fluctuations[1–3] and because of the insight it provides into the spatial structure of turbulent flows. In contrast with single-particle dispersion, which is mostly driven by the large-scale (energy-containing) eddies, the dispersion of pairs of particles depends on velocity fluctuations of order the separation of the pairs. Thus, the early stages of relative dispersion, up to the integral time scale, are expected to reflect the universal nature of small-scale turbulence (independent of the large-scale flow) and the intermittent character of the energy cascade. The latter appears to manifest itself in some particle pairs remaining close together for long periods of time while others separate rapidly.

Clearly, a good understanding of the mechanisms of relative dispersion will lead to better models. Among key features of relative dispersion are a separation-dependent time scale and long-time correlations of quantities such as the relative velocity. Many different types of quantitative models of relative dispersion have been proposed including Lagrangian stochastic models, e.g., Refs. 3–5, and kinematic simulation.[6,7] For a review of relative dispersion and Lagrangian stochastic models in particular, we refer the reader to Sawford.[8] In recent years it has become apparent that the success of these models at small scales will depend on their ability to capture the intermittency of the separation process.[5] One purpose of this paper is to provide a detailed quantitative and qualitative analysis of the separation process which we hope will eventually lead to improved models.

Results from observations of the spread of marked particles (pairs or clouds of tracers in the atmosphere and in the ocean), summarized in classical textbooks such as those by Monin and Yaglom[9] and Pasquill and Smith,[10] are testimony of the difficulty in getting reliable experimental data in fully developed turbulence. Although much progress has been made in recent years in experimental measurements of single Lagrangian particles,[11,12] relatively few Lagrangian measurements have been obtained following pairs of particles. A notable exception is Ott and Mann[13], who report Lagrangian inertial range scaling even at modest Reynolds numbers, of

---

[a]Author to whom correspondence should be addressed. Electronic mail: a.lanotte@isac.cnr.it

TABLE I. Parameters of the numerical simulations: Taylor scale Reynolds number R_λ, root-mean-square velocity u_{rms}, mean energy dissipation ε, viscosity ν, Kolmogorov length scale $\eta=(\nu^3/\varepsilon)^{1/4}$, integral scale L_0, large-eddy turnover time $T_E=L_0/u_{rms}$, Lagrangian velocity autocorrelation time T_L, Kolmogorov time scale $\tau_\eta=(\nu/\varepsilon)^{1/2}$, total integration time T, grid spacing dx, resolution N^3, and number of Lagrangian tracers N_p.

R_λ	u_{rms}	ε	ν	η	L_0	T_E	T_L	τ_η	T	dx	N^3	N_p
183	1.5(1)	0.88(8)	0.002 05	0.01	3.14	2.1	1.3	0.048	5	0.012	512^3	0.96×10^6
284	1.7(1)	0.81(8)	0.000 88	0.005	3.14	1.8	1.2	0.033	4.4	0.006	1024^3	1.92×10^6

the order $R_\lambda \sim 100$, where R_λ is the Taylor scale Reynolds number. As a result, direct numerical simulation (DNS) is still the most important source of detailed Lagrangian statistics (e.g., Refs. 14–18 at Reynolds numbers up to order $R_\lambda \sim 280$). In this paper, we analyze the results of a recent DNS of three-dimensional (3D) homogeneous isotropic turbulence seeded with Lagrangian particles.[19] Although homogeneous isotropic turbulence has limited application to real situations, it is the simplest configuration for studying the statistics of relative dispersion.

The paper is organized as follows. In Sec. II we outline the numerical scheme used for calculating the data and discuss statistical uncertainty and variability. We present results on the statistical properties of both the particle pair separation and its relative velocity. These are considered in Secs. III and IV, respectively. In both cases, we compute the statistics as a function of time and as a function of separation, that is, at fixed scales. The latter allows for a more accurate separation of the dissipative, inertial, and integral scale regions.

II. DNS METHODOLOGY

The direct numerical simulation of homogeneous isotropic turbulence was performed on 512^3 and 1024^3 cubic lattices with Reynolds numbers $R_\lambda \sim 180$ and $R_\lambda \sim 280$, respectively. The Navier-Stokes equations were integrated using fully de-aliased pseudospectral methods for a total time spanning nearly three decades (from the order of a tenth of the Kolmogorov time scale, τ_η, to approximately three times the integral time scale, T_L). The flow was forced by keeping the total energy constant in the first two wavenumber shells.[20] The flow at $R_\lambda=284$ was seeded with approximately two million Lagrangian passive tracers once a statistically stationary velocity field had been obtained. The positions and velocities of the particles were stored at a sampling rate of $0.07\tau_\eta$. The numerical parameters are summarized in Table I. In this DNS, dissipative scales are well resolved, satisfying $\eta \sim dx$, where dx is the grid spacing. The Lagrangian velocity was calculated using linear interpolation, which was demonstrated to be adequate for obtaining well-resolved particle accelerations.[21]

The particles were initially arranged in tetrads which were uniformly distributed in the flow. A total of 960 000 pairs with initial separations $r_0=1.2\eta$ and $r_0=2.5\eta$ were formed this way. Particle pairs with larger initial separations were formed by following pairs chosen from different tetrads. In this way, we also follow pairs with initial separations $r_0=9.8\eta$ and $r_0=19.6\eta$. The number of pairs varied from 5

$\times 10^5$ to 1×10^6 depending on the chosen initial separation. In both cases, a particle may have been used more than once to form a pair.

Previous studies have shown that Lagrangian statistics are affected by highly non-Gaussian fluctuations (see, e.g., Refs. 14 and 18). Thus, it is important to quantify the statistical uncertainty of some typical variable in order to ensure the reliability of the results within our statistical sample. Statistical errors were estimated by dividing the sample into five subensembles and calculating the minimum and maximum values. We find that the error is at worst approximately 15% for the separation skewness and approximately 25% for the relative velocity skewness. The nature of the forcing scheme used in the present DNS meant that relatively little temporal variability of globally averaged quantities was observed (see Overholt and Pope[22] for discussion on forcing schemes and temporal variability). In particular, fluctuations about the mean of the energy dissipation, ε, were at most 10% during the evolution of the DNS. Thus, in the following we may safely use ε (and other globally averaged quantities) to scale the two-particle statistics.

III. SEPARATION STATISTICS

A. Fixed-time statistics

We consider the motion of two marked fluid particles, labeled by the superscripts (1) and (2). In homogeneous turbulence, it is sufficient to consider the statistics of the instantaneous separation of the positions of the two particles, namely $\mathbf{r}(t)=\mathbf{r}^{(1)}(t)-\mathbf{r}^{(2)}(t)$. Furthermore, in isotropic turbulence, the separation magnitude $r=|\mathbf{r}|$ plays a fundamental role in the problem of relative dispersion.

Following the well known ideas of Richardson,[23] relative dispersion in the inertial range of time scales, $\tau_\eta \ll t \ll T_L$, can be modeled in terms of a diffusion equation for the probability density function (PDF) of the pair separation $p(\mathbf{r},t)$. In spherical coordinates this is given by

$$\frac{\partial p(\mathbf{r},t)}{\partial t} = \frac{1}{r^2}\frac{\partial}{\partial r}\left(r^2 K(r)\frac{\partial p(\mathbf{r},t)}{\partial r}\right), \tag{1}$$

where $K(r)$ is a scalar eddy diffusivity. On the basis of experimental measurements in the atmosphere, Richardson proposed that $K(r)=k_0\varepsilon^{1/3}r^{4/3}$, where k_0 is a dimensionless constant. Assuming a small enough initial separation and a large enough travel time, it can be shown (see, e.g., Monin and Yaglom,[9] p. 574) that a spherically symmetric solution of (1) is given by
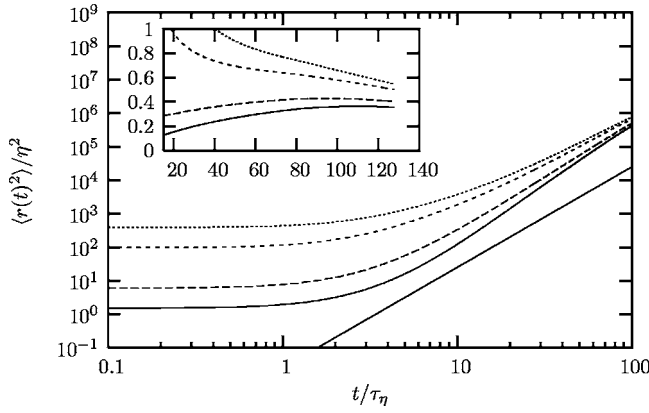
FIG. 1. The evolution of $\langle r(t)^2 \rangle / \eta^2$ vs t/τ_η for the initial separations $r_0 = 1.2\eta$, $r_0 = 2.5\eta$, $r_0 = 9.8\eta$, and $r_0 = 19.6\eta$. The straight line is proportional to t^3. Inset: $\langle r(t)^2 \rangle / \varepsilon t^3$ for the same four initial separations starting from $t/\tau_\eta \sim 15$.
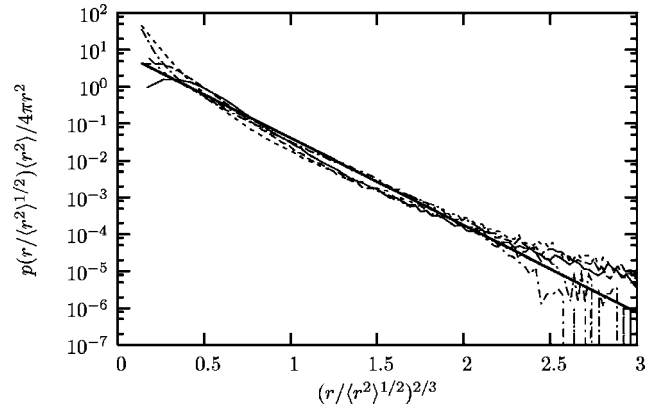

FIG. 2. Comparison of the Richardson PDF with the DNS data. The curves refer to data for $r_0 = 1.2\eta$ at $t = 5.2\tau_\eta$ (solid line), $t = 7\tau_\eta$ (long dashed line), $t = 14\tau_\eta$ (short dashed line), $t = 42\tau_\eta$ (dotted line), and $t = 70\tau_\eta$ (dot-dashed line). The thick solid line is the Richardson PDF (2).

$$p(r,t) = \frac{Ar^2}{(k_0 \varepsilon^{1/3} t)^{9/2}} \exp\left(-\frac{9r^{2/3}}{4k_0 \varepsilon^{1/3} t}\right), \qquad (2)$$

where $A = (3/2)^8 / \Gamma(9/2)$ is a normalization constant. This exhibits strong non-Gaussianity with a narrow peak at the origin and very large tails and gives rise to the celebrated scaling for the second-order moment

$$\langle r^2 \rangle = g\varepsilon t^3. \qquad (3)$$

Here $g = 1144 k_0^3 / 81$ is the Richardson constant which is supposed to be universal. This result was also derived by Obukhov[24] using Kolmogorov's classical theory of turbulence (K41).[9]

The Richardson PDF is perfectly self-similar; all positive moments behave according to the dimensional law $r^p \propto t^{3p/2}$. The scaling (3) is notoriously difficult to achieve both in laboratory experiments and in DNS on account of the large separation of scales that is required to observe it. As a result, estimates of g have varied widely, from 0.06 to 3.5.[8] The main practical difficulties in achieving a long inertial subrange are due to dissipative range effects at the ultraviolet end of the spectrum, integral scale effects at the infrared end of the spectrum, and the finite initial separation of the pairs. In the dissipation range, pairs separate exponentially and with widely varying growth rates—some pairs separate rapidly while others remain close together. This leads to the formation of a broad distribution of separations. As a result, slowly separating pairs (which remain in the dissipative range) and rapidly separating pairs (which approach the integral scales) "contaminate" the statistics in the inertial range. A very large Reynolds number is therefore required to produce reliable Lagrangian statistics in the inertial range.

In Fig. 1 we plot the mean-square separation $\langle r^2 \rangle$ vs t, normalized by the Kolmogorov microscales, η and τ_η, respectively. Although the curves begin to collapse at large t, they do not display a t^3 scaling and still show a dependence on the initial separation. Thus, any attempt to extract the value of the Richardson constant will be marred by the memory of the initial separation. The simplest way to measure g is to plot $\langle r^2 \rangle$ scaled by the asymptotic prediction, εt^3,

and look for a plateau. These curves are displayed in the inset of Fig. 1. It is clear that none of them produces a good plateau, and, given the spread of curves with different initial separations, the value will be at best an order of magnitude estimate subject to considerable uncertainty.

An alternative method, used in Refs. 13, 15, and 18, consists of fitting a straight line to $\langle r^2 \rangle^{1/3}$ in a suitable time interval. If Eq. (3) holds, this straight line, when extrapolated back toward $t = 0$, should pass through the origin and have a slope of $(g\varepsilon)^{1/3}$. For all curves, we find a small nonzero intercept whose value varies with r_0. This introduces an extra free parameter in the linear fit corresponding to the nonzero intercept. The curve with the smallest nonzero intercept has $r_0 = 2.5\eta$ and gives a value of $g = 0.47$ with an error of the order of approximately 10% depending on the time range (here taken to be $15\tau_\eta \lesssim t \lesssim 75\tau_\eta$). This value of g is smaller than that found by Yeung and Borgas[18] and Ishihara and Kaneda,[15] though still of the same order of magnitude, but agrees well with that of Ott and Mann[13] and Boffetta and Sokolov.[14]

In order to make a more complete analysis of Richardson's model, we compute the PDF of the separation distance. The Richardson PDF relies on two phenomenological assumptions: the first is that the eddy diffusivity is self-similar, the second is that the velocity field is short-time correlated. However, it is known that anomalous corrections to the K41 scalings exist (see, e.g., Ref. 25), and these are likely to complicate the situation.

In Fig. 2 we compare the separation PDF for the smallest initial separation, $r_0 = 1.2\eta$, calculated from the DNS data, with that predicted by Richardson, namely (2). For small times (up to $t \sim 40\tau_\eta$), we observed a rapid change in shape with the PDF showing a pronounced tail, which indicates that while most pairs are still close together, some have moved very far apart (not shown). At these times the curves do not rescale, indicating that the early stages of the separation process are very intermittent. Here, the physics of the dissipative range still exerts an influence on the separation process and so we would not expect agreement with the Richardson PDF. Only for times in the range 40–$70\tau_\eta$ do we
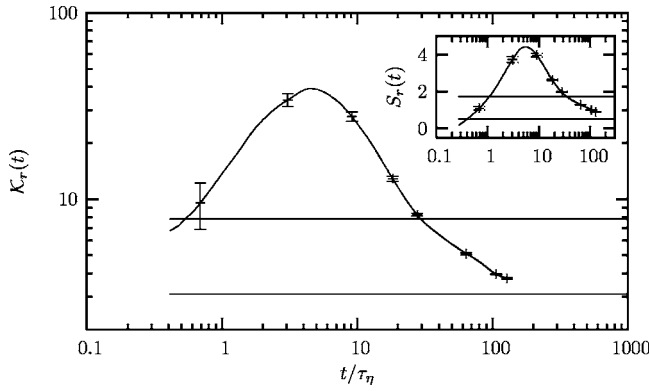
FIG. 3. The separation kurtosis for the smallest initial separation $r_0=1.2\eta$. Also shown at some times are the error bars calculated from the minimum and maximum values of the five subensembles. Inset: the separation skewness for the same initial separation together with the error bars at the same times. The horizontal lines are the appropriate values derived from the Richardson PDF and the chi-squared distribution with three degrees of freedom. These values are 1.7 and 0.49, respectively, for the skewness and 7.81 and 3.1, respectively, for the kurtosis.

FIG. 4. The normalized correlation function $R(t,\tau)/R(t,0)$ vs τ/t for $r_0=1.2\eta$ at different travel times. Inset: the same correlation functions now plotted vs τ/τ_η with $-t\leqslant\tau\leqslant0$. Curves (from left to right) refer to travel times $t=77\tau_\eta$, $t=63\tau_\eta$, $t=49\tau_\eta$, $t=35\tau_\eta$, and $t=21\tau_\eta$.

find reasonable agreement with the Richardson PDF. We note that while at $t\sim40\tau_\eta$ we find good agreement for the tail but a large mismatch for values close to the peak, at $t\sim70\tau_\eta$ the PDF is almost indistinguishable from (2). At large times, the particles are moving more or less independently and so the PDF of r^2 will be a chi-squared distribution with three degrees of freedom (not shown).

A more detailed analysis of the separation PDF can be made by considering the separation skewness, $S_r(t)=\langle[r(t)-\overline{r(t)}]^3\rangle/[\sigma_r^2(t)]^{3/2}$, and the kurtosis, $\mathcal{K}_r(t)=\langle[r(t)-\overline{r(t)}]^4\rangle/[\sigma_r^2(t)]^2$, where $\overline{r}$ is the mean separation distance and σ_r is the root-mean-square separation distance. These are shown in Fig. 3 for $r_0=1.2\eta$ and clearly show the intermittent nature of the separation process at small times, in agreement with that found by Yeung and Borgas.[18] The Richardson PDF, of course, predicts constant values for the skewness and kurtosis, namely 1.7 and 7.81, respectively, and which are not reached until approximately $t\sim35\tau_\eta$. This time is within the inertial subrange and we may have expected the skewness and kurtosis to level off before decreasing to their large time values (0.49 and 3.1, respectively). That this is clearly not the case suggests that either contamination of the inertial range due to the dissipative and integral scales prevents us from having a region of constant skewness and kurtosis, or there are shortcomings in the Richardson model.

These results put the difficulties of calculating Richardson's constant (described above) into context. A perfect collapse of curves in the PDF would have implied self-similarity, but its absence is not necessarily an indication of the failure of the Richardson model; as we have already discussed, each end of the inertial range is affected by, respectively, dissipation range and integral scale effects. In Sec. III B, we show how these problems may be overcome by measuring statistics at fixed scales.

We conclude this section by considering the correlation function $R(t,\tau)=\langle r(t)r(t+\tau)\rangle$ of the separation distance for travel times within the inertial subrange. This quantity, which probes two differen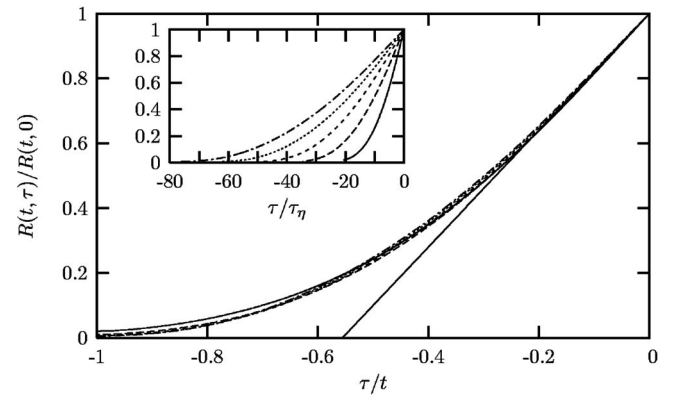t times along the separation process, is influenced by the temporal properties of the turbulent energy cascade sustaining the separation growth. In the inset of Fig. 4 we plot $R(t,\tau)$ for $-t\leqslant\tau\leqslant0$ at different travel times t for pairs with initial separation $r_0=1.2\eta$. In agreement with Jullien *et al.*,[26] we find that $R(t,\tau)$ broadens with increasing travel time, indicating that the pairs decorrelate more slowly at larger travel times, a consequence of the fact that larger and larger eddies have slower and slower dynamics. In the body of the figure, we plot the same data versus τ/t. Dimensional analysis, based on the assumption that the correlation function decays with the eddy turn over time at scale r, shows that $R(t,\tau)/R(t,0)=f(\tau/t)$. The collapse of all curves onto a single one supports the above dimensional prediction and tells us that, notwithstanding that the pair separation is a nonstationary process in the Lagrangian framework, there is a single correlation function which applies to the whole inertial range.

B. Fixed-scale statistics

To disentangle the effects of different scales, an alternative approach, based on *exit time* statistics, has been proposed.[27] This consists of fixing a set of thresholds, $r_n=\rho^n r_0$, where $\rho>1$ and $n=1,2,3,\ldots$, and then calculating the time T taken for the pair separation to change from r_n to r_{n+1}. By averaging over the particle pairs, we obtain the mean exit time, $\langle T_\rho(r_n)\rangle$, or mean *doubling time* if $\rho=2$. Formally, we are calculating the first passage time. The advantage of this approach is that all pairs are sampled at the same scales and that finite Reynolds number effects are less important.[27] For particle pairs with initial condition $p(\mathbf{r},0)=\rho^2\delta(r-r_n/\rho)/4\pi r_n^2$, and an absorbing boundary condition at $r=r_n$, the PDF of the exit time, T, is defined to be

$$\mathcal{P}_{\rho,r_n}(T)=-\frac{\mathrm{d}}{\mathrm{d}T}\int_{|\mathbf{r}|<r_n}p(\mathbf{r},T)\mathrm{d}\mathbf{r}, \tag{4}$$
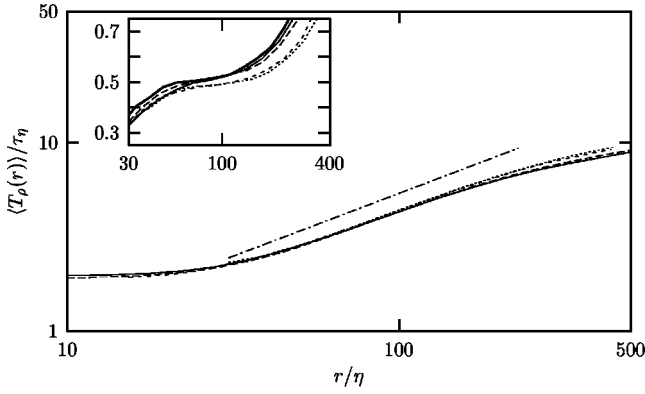
from which we get

FIG. 5. The mean exit time for the initial separations $r_0=1.2\eta$ (thin continuous line), $r_0=2.5\eta$ (long dashed line), $r_0=9.8\eta$ (short dashed line), and $r_0=19.6\eta$ (dotted line) with $\rho=1.25$. The straight line is proportional to $r^{2/3}$. In the inset we show Richardson's constant, g, vs r/η as given by (9) for the same initial separations at $R_\lambda=284$. To evaluate the variability of g with the Reynolds number, we also plot a curve (thick continuous line) for the initial separation $r_0=1.2\eta$ at $R_\lambda=183$.
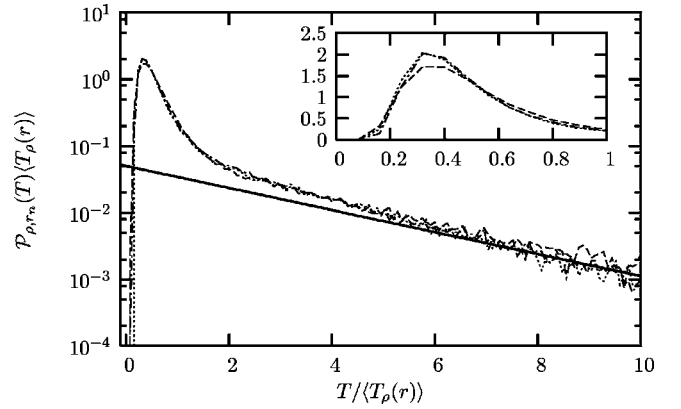

FIG. 6. The log-linear plot of the exit time PDF for $r_0=1.2\eta$ with $\rho=1.25$ at $r=21.8\eta$ (dashed line), $r=83.3\eta$ (dotted line), and $r=130.1\eta$ (dot-dashed line). The solid line is the large time prediction (10). Inset: a lin-lin plot of the same figure showing more detail.

$$\mathcal{P}_{\rho,r_n}(T) = -4\pi k_0 \varepsilon^{1/3} r_n^{10/3} \frac{\partial p}{\partial r}\bigg|_{r=r_n}, \tag{5}$$

on making use of (1). Following Boffetta and Sokolov,[28] we can derive a solution of the 3D diffusion equation (1) in terms of an eigenfunction decomposition. This gives us

$$p(\xi,t) = \sum_{i=1}^{\infty} c_i \exp(-\lambda_i^2 t)\xi^{-7/2} J_{7/2}(3\lambda_i \xi), \tag{6}$$

where $\xi=(k_0\varepsilon^{1/3})^{-1/2}r^{1/3}$, $J_{7/2}(x)$ is a Bessel function of the first kind, $\lambda_i=1/3(k_0\varepsilon^{1/3})^{1/2}r^{-1/3}j_{7/2,i}$, where $j_{7/2,i}$ are the zeros of $J_{7/2}(x)$ and c_i are constants. It then follows from (5) that the large-time asymptotic form of the exit time PDF is given by

$$\mathcal{P}_{\rho,r_n}(T) \sim \exp\left(-\kappa \frac{2k_0\varepsilon^{1/3}}{r_n^{2/3}}T\right), \tag{7}$$

where $\kappa \approx 2.72$ is a numerical constant derived from the leading zero of the Bessel function described above.

Using Richardson's diffusion equation (1), the mean exit time can be shown to be[14]

$$\langle T_\rho(r_n)\rangle = \frac{1}{2k_0}\frac{\rho^{2/3}-1}{\rho^{2/3}}\frac{r_n^{2/3}}{\varepsilon^{1/3}}. \tag{8}$$

In the body of Fig. 5 we plot $\langle T_\rho(r_n)\rangle$ for a range of initial separations. It is immediately clear that there is no dependence on the initial separation in contrast to the mean-square separation calculated as a function of time (see Fig. 1). Moreover, we see a much clearer inertial scaling region in which the mean exit time grows almost like $r^{2/3}$.

Equation (8) provides us with a method for calculating the Richardson constant (since k_0 is related to g):

$$g = \frac{143}{81}\frac{(\rho^{2/3}-1)^3}{\rho^2}\frac{r^2}{\varepsilon\langle T_\rho(r)\rangle^3}. \tag{9}$$

In the inset of Fig. 5, we plot the expression (9) for the Richardson constant versus r for various initial conditions.

We see that a collapse of curves is beginning to form for all initial separations. We estimate the value of g to be approximately 0.50 ± 0.05, which agrees with the value computed above and with previous estimates of g.[13,14,29] This method has the advantage of relative insensitivity to the initial separation and avoids the problem of the nonzero intercept discussed in Sec. III A. Of course, the present calculation of g assumes the validity of Richardson's model. We find that g does not change significantly for $\rho \in [1.15,2]$. It is also worth noticing that the estimate of g is not very sensitive to the Reynolds number (see the inset of Fig. 5).

The exit time PDF, $\mathcal{P}_{\rho,r_n}(T)$, is shown in Fig. 6 for $r_0=1.2\eta$ and clearly shows the exponential nature of the exit time PDF at large times. At intermediate and large exit times, $T_\rho(r_n) \gtrsim \langle T_\rho(r_n)\rangle$, the exit time PDF agrees well with the theoretical prediction (7), when reexpressed in a universal form using the mean exit time (8):

$$\mathcal{P}_{\rho,r_n}(T) \sim \exp\left(-\kappa \frac{\rho^{2/3}-1}{\rho^{2/3}}\frac{T}{\langle T_\rho(r_n)\rangle}\right). \tag{10}$$

The clear collapse of curves for $T_\rho(r_n) \gtrsim \langle T_\rho(r_n)\rangle$ indicates that the exit time statistics in this range are self-similar (although we note that the collapse deteriorates with increasing ρ). The deterioration of the collapse at very large exit times is due to statistical noise—there are relatively few pairs which remain close together for long periods of time. Here we have shown that by focusing on statistics at fixed scales, such that the effect of the infrared and ultraviolet cutoffs on the inertial range is reduced and the finite initial separation of the particle pairs becomes unimportant, the Richardson diffusion model appears to work well for the inertial range of scales. For small exit times, $T_\rho(r_n) \ll \langle T_\rho(r_n)\rangle$, on the other hand, we do not find a complete collapse of curves at different thresholds, indicating that rapidly separating pairs are likely to exhibit intermittency (see the inset of Fig. 6).

The higher-order moments of T are dominated by those pairs which separate slowly. Conversely, the moments of the inverse exit times, $\langle [1/T_\rho(r)]^p\rangle$, are dominated by those pairs
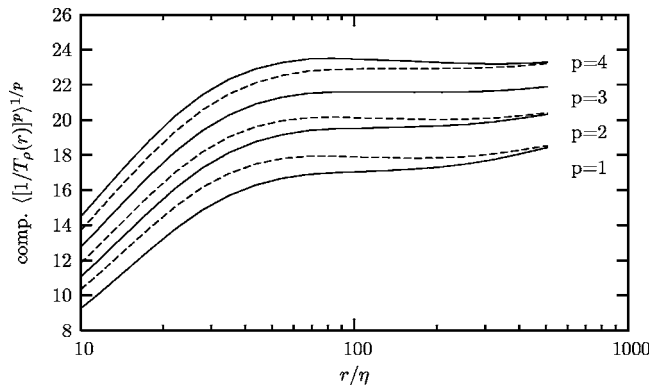
FIG. 7. The inverse exit time moments, $\langle[1/T_\rho(r)]^p\rangle^{1/p}$, for $p=1,\ldots,4$ compensated with the Kolmogorov scalings (solid lines) and the multifractal predictions (dashed lines) for the initial separation $r_0=1.2\eta$ and for $\rho=1.25$.

FIG. 8. The finite-size Lyapunov exponents as a function of the separation r_n for different Reynolds numbers.

which separate rapidly and correspond to positive moments of the separation. Kolmogorov scaling based on dimensional analysis then leads to

$$\left\langle\left(\frac{1}{T_\rho(r)}\right)^p\right\rangle \sim \varepsilon^{p/3} r^{-2p/3}. \tag{11}$$

Assuming that a reasonable estimate of the exit time is given by $T(r)\sim r/u_r$, where u_r is the relative velocity at scale r, intermittency corrections can be quantified in terms of the multifractal formalism,[30]

$$\left\langle\left(\frac{1}{T_\rho(r)}\right)^p\right\rangle \sim \frac{1}{T_L^p}\left(\frac{r}{L_0}\right)^{\zeta_E(p)-p}, \tag{12}$$

where $\zeta_E(p)$ are the scaling exponents of the Eulerian velocity structure functions as predicted by the multifractal formalism. In Fig. 7, we plot $\langle[1/T_\rho(r)]^p\rangle^{1/p}$ scaled by the Kolmogorov scaling exponents (11) and intermittent scaling exponents (12), respectively. The $\zeta_E(p)$ are calculated using the She-Lévêque formula.[31] As already remarked at lower Reynolds numbers by Boffetta and Sokolov,[14] there is a small but clear improvement in the scaling of the inverse exit times when scaled by the multifractal predictions.

Before concluding this section, we note that the exit time statistics can be used to measure the largest Lyapunov exponent in the flow. This is because for small thresholds, r_n, the mean exit time probes the exponential growth of the separation distances. The exact relation between the "finite size Lyapunov exponent" and the mean exit time is[32]

$$\lambda = \lim_{r_n\to 0}\frac{1}{\langle T_\rho(r_n)\rangle}\log(\rho). \tag{13}$$

In Fig. 8, we show the right-hand side of (13) for three different Reynolds numbers (two from this numerical simulation, see Table I) and one from a previous DNS study,[14] at different thresholds, r_n. The usual Lyapunov exponent is recovered from the saturation value in the limit of small r_n. As may be seen in the figure, the data show a clear proportionality between the Kolmogorov time, τ_η, and the Lyapunov exponents, λ, for all available Reynolds numbers. Thus, we get
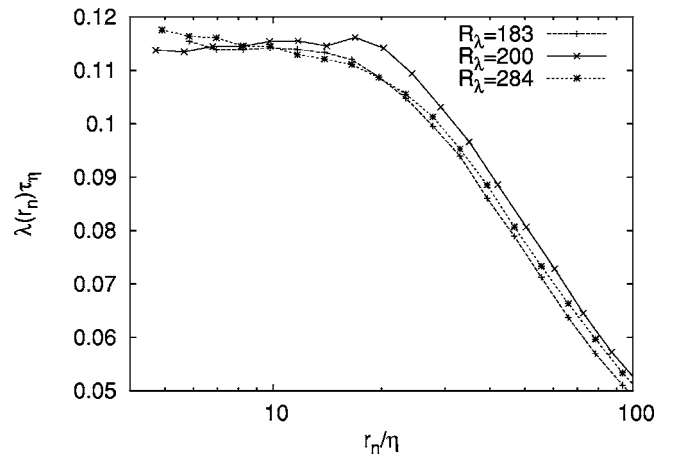
$$\lambda\tau_\eta \sim 0.115 \pm 0.005.$$

This value is comparable with the one found by Girimaji and Pope.[33]

IV. RELATIVE VELOCITY STATISTICS

A. Fixed-time statistics

We now consider the statistics of the relative velocity of the particle pairs during the separation process and which we denote as $\mathbf{u}_r(t)=\mathbf{u}^{(1)}(t)-\mathbf{u}^{(2)}(t)$. The relative velocity statistics are of interest because they provide information on the rate of separation of the particle pairs. We consider the statistics of the relative velocity projected in the direction of the separation vector, the "longitudinal" component, and the projection of the relative velocity orthogonal to the separation, the "transverse" component. The former is given by

$$u_\parallel = \frac{dr}{dt} = \mathbf{u}_r\cdot\hat{\mathbf{r}},$$

where $\hat{\mathbf{r}}=\mathbf{r}/r$. The transverse component of the relative velocity is given by

$$\mathbf{u}_\perp = \mathbf{u}_r - u_\parallel\hat{\mathbf{r}}.$$

There are, of course, two transverse components of the relative velocity, but since the turbulence is isotropic it suffices to consider only one. We comment here that the relative magnitudes of $\langle|\mathbf{u}_r|\rangle$, $\langle|u_\parallel|\rangle$, and $\langle|\mathbf{u}_\perp|\rangle$ and the alignment properties of $\mathbf{u}_r$, $\mathbf{r}(t)$, and $\mathbf{r}(0)$ have been discussed extensively by Yeung and Borgas.[18] Here, we state simply that our data give similar results and concentrate on the PDFs of the velocity components and their properties.

In Fig. 9 we plot the PDF of the longitudinal component of the relative velocity, $u_\parallel(t)$, for $r_0=1.2\eta$. The PDF is negatively skewed at $t=0$ (not shown), corresponding to the Eulerian distribution, but as t increases, it quickly becomes positively skewed, indicating that pairs with small initial separation are more likely to be diverging than converging. This skewness then decreases and the PDF tends toward a Gaussian distribution for travel times of order T_L. The PDF of one component of $\mathbf{u}_\perp$ for the same initial separation is
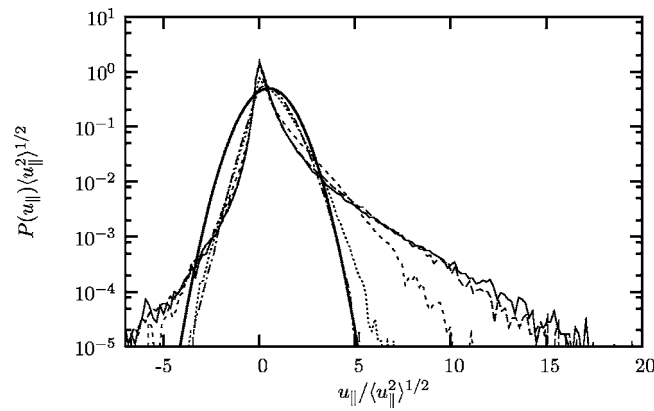
FIG. 9. The PDF of $u_\parallel$ for $r_0 = 1.2\eta$ at the following travel times (from outer to inner curve): $t = 5.2\tau_\eta$, $t = 7\tau_\eta$, $t = 14\tau_\eta$, $t = 42\tau_\eta$, and $t = 70\tau_\eta$. The thick solid line is a Gaussian distribution.

FIG. 11. The kurtosis of $u_\parallel$ (continuous line) and of $u_\perp$ (dashed line) for the smallest initial separations $r_0 = 1.2\eta$. Inset: the skewness of $u_\parallel$ for the same initial separation. The horizontal lines are the Gaussian values for the kurtosis and skewness.

shown in Fig. 10. Unlike the PDF of $u_\parallel$, it is symmetric about the mean. Thus, negative velocities are as common as positive velocities indicating that there is no preferred direction of rotation as may be expected in isotropic and parity invariant turbulence. We note here that for both longitudinal and transverse PDFs we do not see a complete collapse of curves for times in the range $t \in [10, 70]\tau_\eta$.

We consider the PDFs of the relative velocity components in more detail by analyzing their skewness $S_u(t)$ and kurtosis $\mathcal{K}_u(t)$. These are shown in Fig. 11 for $r_0 = 1.2\eta$, and compare well with the results reported in Ref. 18. At $t = 0$, the Lagrangian statistics (not shown) are identical to the Eulerian statistics. This is reflected in the negative skewness of $u_\parallel$, which is close to -0.55, the value commonly observed for Eulerian velocity structure functions at moderate to high Reynolds numbers.[34] We also note that at early times (up to $t \sim 10\tau$) the maximum values of the skewness and kurtosis of the velocity statistics are higher than the corresponding maxima of the separation statistics. We conclude this section by measuring the correlation of the relative velocity along the particle pair trajectories. In the inset of Fig. 12 we plot $D(t, \tau) = \langle u_\parallel(t) u_\parallel(t+\tau) \rangle$ for $-t \le \tau \le 0$ for pairs with initial separation $r_0 = 1.2\eta$. In agreement with Fig. 4 we find that $D(t, \tau)$ broadens with increasing travel time, confirming that
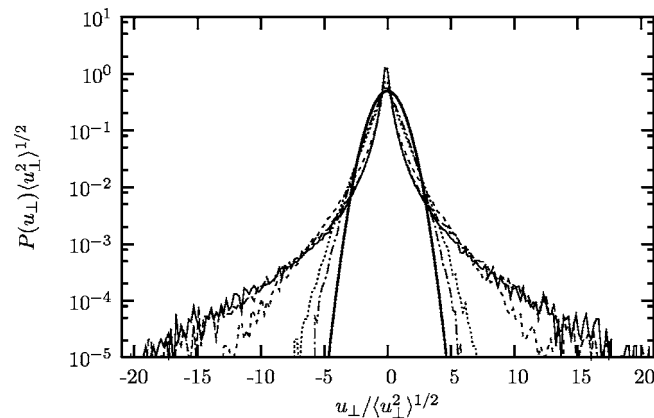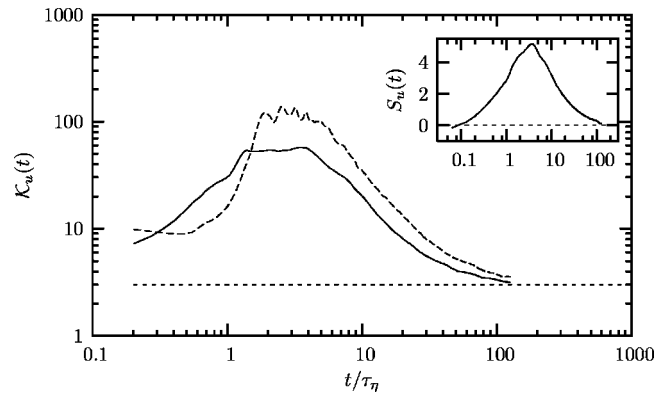
the velocity decorrelates more slowly at larger travel times. In the body of the same figure we plot the same data rescaled versus τ/t. We note here that the rescaling does not give as good a collapse as for the separation statistics. This may be due to the finite size of the inertial subrange or the presence of *tiny* anomalous fluctuations in the characteristic times governing the decorrelation of eddies of different size.

B. Fixed-scale statistics

Following the exit time method of Sec. III B, we calculate the relative velocity at fixed scales in order to achieve "uncontaminated" inertial range statistics and which we term the *exit velocities*. We compute the value of the relative velocity components $u_\parallel(r)$ and $\mathbf{u}_\perp(r)$ whenever a particle pair has a separation within a specified logarithmic shell of radius $r = r_n(1 \pm 0.1)$, with $r_n = \rho^n r_0$. This differs from the method we used to calculate the exit times above as here we are calculating not just the velocity at the first passage but also at all subsequent passages.

In Fig. 13 we plot the mean longitudinal exit velocity, $\langle u_\parallel(r) \rangle$, as a function of the absolute separation, r, for different r_0. The lack of dependence on r_0 is immediately apparent. We also see a clear separation between dissipative and
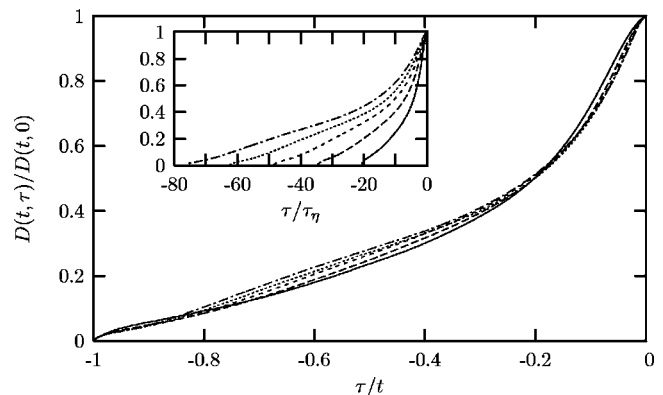

FIG. 10. The PDF of $u_{\perp z}$ for $r_0 = 1.2\eta$ at the same times as Fig. 9. The thick solid line is a Gaussian distribution.

FIG. 12. The normalized correlation function $D(t, \tau)/D(t, 0)$ vs τ/t and τ/τ_η (inset) for pairs with initial separation $r_0 = 1.2\eta$. Curves (from left to right) refer to travel times $t = 77\tau_\eta$, $t = 63\tau_\eta$, $t = 49\tau_\eta$, $t = 35\tau_\eta$, and $t = 21\tau_\eta$.
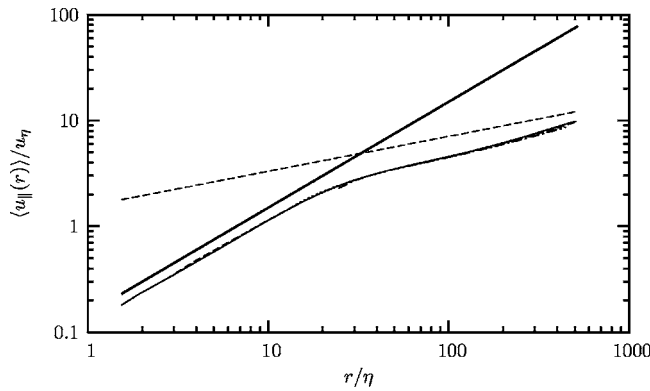
FIG. 13. The mean longitudinal exit velocity, $\langle u_\parallel \rangle$, as a function of the separation and scaled by $u_{\eta'} = \eta / \tau_\eta$, for pairs with initial separations $r_0 = 1.2\eta$, $r_0 = 2.5\eta$, $r_0 = 9.8\eta$, and $r_0 = 19.6\eta$. The thick solid line is proportional to r and the dashed line is proportional to $r^{1/3}$.

FIG. 15. The log-lin plot of the exit velocity PDF $\mathcal{P}(u_{\perp z})$ for $r_0 = 1.2\eta$, at the same thresholds as Fig. 14. The thick solid line is a Gaussian distribution.

inertial range scales, with $\langle u_\parallel \rangle$ growing linearly for small r, corresponding to the dissipation range and then growing close to $r^{1/3}$ for larger r, which corresponds to the inertial range. Similar behavior was observed for $|\mathbf{u}_\perp(r)|$. However, the very existence of a nonvanishing mean longitudinal relative velocity tells us that the two sets of statistics cannot be identical. We consider these differences in more detail by analyzing the PDFs of the exit velocities.

In Fig. 14 we plot the PDF of the longitudinal (exit) velocity, $\mathcal{P}(u_\parallel)$, and in the inset we plot $u_\parallel^4 \mathcal{P}(u_\parallel)$. In contrast to the Eulerian PDF, the PDF is slightly positively skewed initially, but as the separation threshold increases it becomes more symmetric and tends toward a Gaussian distribution. However, unlike the PDF of $u_\parallel(t)$ (see Fig. 9), we do not see an initial rapid increase in the positive tail of the PDF. At fixed separations there is not the spread of contributions to the velocity as there is at fixed times. The PDF of one component of the transverse relative exit velocity, $\mathcal{P}(u_{\perp z})$, is shown in Fig. 15 for the same initial separation $r_0 = 1.2\eta$. As may be expected, this PDF is initially symmetric and remains so for increasing separation threshold. The absence of
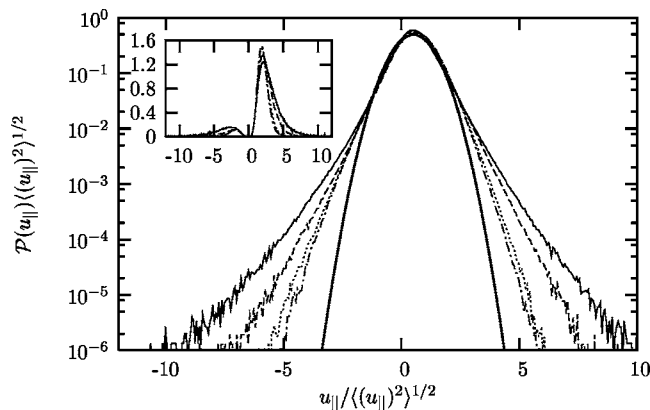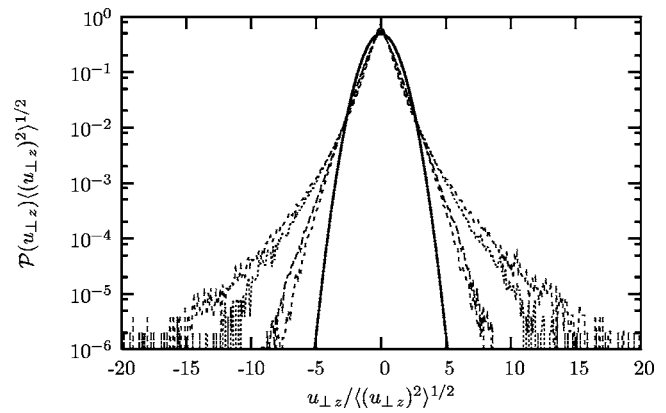
a complete collapse of curves at different thresholds in both PDFs indicates that the exit velocities are intermittent.

We examine the intermittency of the exit velocities by considering their second- and fourth-order moments. Since the exit velocity statistics resemble Eulerian velocity statistics, we use the multifractal formalism for Eulerian velocity structure functions to quantify the intermittency corrections. In this way, we have a reasonable estimate to compare with. The Eulerian structure functions scale according to $\langle \delta_r v \rangle \sim (r/L_0)^{\zeta_E(p)}$ (see, e.g., Ref. 25). The She-Lévêque formula for the scaling exponents, $\zeta_E(p)$, gives $\zeta_E(2) = 0.7$ and $\zeta_E(4) = 1.28$. Figure 16 shows that the second-order moment of both the longitudinal and transverse relative velocity components scales according to the multifractal prediction. For the fourth-order moment we find that the transverse component scales well with the multifractal prediction but the longitudinal component shows a small discrepancy.

V. CONCLUSION

We have considered the separation process of particle pairs in homogeneous isotropic turbulence in considerable detail. In addition to presenting such classical but important statistics as the PDF of the separation distance and its
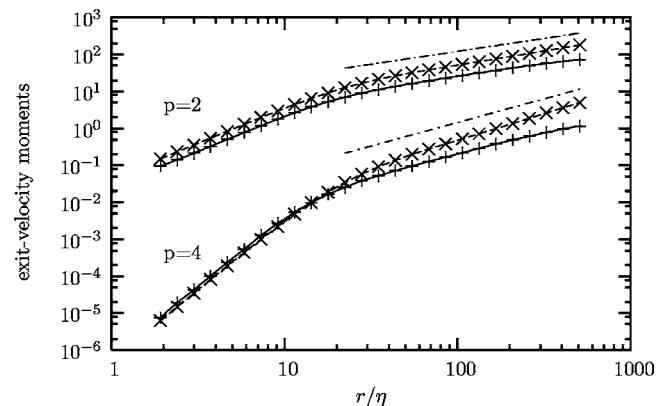

FIG. 14. The log-lin plot of the exit velocity PDF $\mathcal{P}(u_\parallel)$ calculated as a function of r for pairs with $r_0 = 1.2\eta$. The curves are for the following thresholds: $r = 5.72\eta$, $r = 21.8\eta$, $r = 83.3\eta$, and 130.1η (from outer to inner curve). The thick solid line is a Gaussian distribution. Inset: a lin-lin plot of $u_\parallel^4 \mathcal{P}(u_\parallel)$.

FIG. 16. The second- and fourth-order exit velocities for the longitudinal $u_\parallel$ ($\times$ symbol) and transverse $u_{\perp z}$ ($+$ symbol) relative velocities for $r_0 = 1.2\eta$. The dot-dashed lines are the multifractal prediction for the second- and fourth-order moments.

second-order moment (which gives us Richardson's constant), we also considered higher order moments of the separation. Here, in agreement with Ref. 18, we found very high levels of the kurtosis and skewness at small times for pairs with small initial separation. A quantitative assessment of this intermittency in the inertial subrange was made difficult by the contamination of the inertial subrange by dissipation range and integral scale effects. In order to get a clearer separation between the dissipation range, inertial subrange, and integral scales, we computed the statistics at fixed separations, the *exit time* statistics. This provided us with an alternative method for calculating Richardson's constant, the value of which agreed well with the "direct" method. Moreover, these statistics allowed us to estimate intermittency corrections quantitatively in terms of the multifractal formalism. In agreement with Boffetta and Sokolov,[14] we found a small but noticeable deviation from self-similar behavior for those pairs that separate rapidly. The multifractal model—an inertial subrange model—better captures the anomalous scaling exhibited by these pairs.

We also calculated the longitudinal and transverse components of the relative velocity as a function of both travel time and the separation, that is, the *exit velocities*. Analogous to the separation statistics, we found that dissipation range and integral scale effects made a quantitative assessment of intermittency corrections difficult in the inertial subrange for the Lagrangian statistics computed as a function of time. However, the fixed-scale approach showed a clear separation of scales with the velocities scaling like the Eulerian velocity structure functions (for moments up to order 4). These statistics allowed us to quantify intermittency corrections in terms of the multifractal model for Eulerian velocity structure functions. However, we also noted a small but significant difference with the true Eulerian statistics for the case of the longitudinal exit velocity.

ACKNOWLEDGMENTS

[1] G. K. Batchelor, "Diffusion in a field of homogeneous turbulence. II. The relative motion of particles," Proc. Cambridge Philos. Soc. **48**, 345 (1952).
[2] P. A. Durbin, "A stochastic model of two-particle dispersion and concentration fluctuations in homogeneous turbulence," J. Fluid Mech. **100**, 279 (1980).
[3] D. J. Thomson, "A stochastic model for the motion of particle pairs in isotropic high-Reynolds-number turbulence, and its application to the problem of concentration variance," J. Fluid Mech. **210**, 113 (1990).
[4] O. A. Kurbanmuradov, "Stochastic Lagrangian models of two-particle relative turbulent dispersion in high-Reynolds number turbulence," Monte Carlo Meth. Appl. **3**, 37 (1997).
[5] M. S. Borgas and P. K. Yeung, "Relative dispersion in isotropic turbulence: Part 2. A new stochastic model with Reynolds number dependence," J. Fluid Mech. **503**, 125 (2004).
[6] N. A. Malik and J. C. Vassilicos, "A Lagrangian model for turbulent dispersion with turbulent-like flow structure: Comparison with direct numerical simulation for two-particle statistics," Phys. Fluids **11**, 1572 (1999).
[7] J. C. H. Fung and J. C. Vassilicos, "Two-particle dispersion in turbulent-like flows," Phys. Rev. E **57**, 1677 (1998).
[8] B. L. Sawford, "Turbulent relative dispersion," Annu. Rev. Fluid Mech. **33**, 289 (2001).
[9] A. S. Monin and A. M. Yaglom, *Statistical Fluid Mechanics* (MIT Press, Cambridge, MA, 1975), Vol. 2.
[10] F. Pasquill and F. B. Smith, *Atmospheric Diffusion* (Ellis Horwood, Chichester, 1983).
[11] N. Mordant, P. Metz, O. Michel, and J.-P. Pinton, "Measurement of Lagrangian velocity in fully developed turbulence," Phys. Rev. Lett. **87**, 214501 (2001).
[12] A. La Porta, G. A. Voth, A. M. Crawford, J. Alexander, and E. Bodenschatz, "Fluid particle accelerations in fully developed turbulence," Nature (London) **409**, 1017 (2001).
[13] S. Ott and J. Mann, "An experimental investigation of the relative diffusion of particle pairs in three-dimensional turbulent flow," J. Fluid Mech. **422**, 207 (2000).
[14] G. Boffetta and I. M. Sokolov, "Relative dispersion in fully developed turbulence: The Richardson's law and intermittency corrections," Phys. Rev. Lett. **88**, 094501 (2002).
[15] T. Ishihara and Y. Kaneda, "Relative dispersion of a pair of fluid particles in the inertial subrange of turbulence," Phys. Fluids **14**, L69 (2002).
[16] P. K. Yeung, "Direct numerical simulation of two-particle relative diffusion in isotropic turbulence," Phys. Fluids **6**, 3416 (1994).
[17] P. K. Yeung, "One- and two-particle Lagrangian acceleration correlations in numerically simulated homogeneous turbulence," Phys. Fluids **9**, 2981 (1997).
[18] P. K. Yeung and M. S. Borgas, "Relative dispersion in isotropic turbulence: Part 1. Direct numerical simulations and Reynolds number dependence," J. Fluid Mech. **503**, 93 (2004).
[19] L. Biferale, G. Boffetta, A. Celani, A. Lanotte, and F. Toschi, "Particle trapping in three dimensional fully developed turbulence," Phys. Fluids **17**, 021701 (2005).
[20] S. Chen, G. D. Doolen, R. H. Kraichnan, and Z. S. She, "On statistical correlations between velocity increments and locally averaged dissipation in homogeneous turbulence," Phys. Fluids A **5**, 458 (1993).
[21] L. Biferale, G. Boffetta, A. Celani, B. J. Devenish, A. Lanotte, and F. Toschi, "Multifractal statistics of Lagrangian velocity and acceleration in turbulence," Phys. Rev. Lett. **93**, 064502 (2004).
[22] M. R. Overholt and S. B. Pope, "Direct numerical simulation of a passive scalar with imposed mean gradient in isotropic turbulence," Phys. Fluids **8**, 3128 (1996).
[23] L. F. Richardson, "Atmospheric diffusion shown on a distance-neighbour graph," Proc. R. Soc. London, Ser. A **110**, 709 (1926).
[24] A. Obukhov, "Spectral energy distribution in a turbulent flow," Izv. Akad. Nauk SSSR, Ser. Geogr. Geofiz. **5**, 453 (1941).
[25] U. Frisch, *Turbulence: The Legacy of A. N. Kolmogorov* (Cambridge University Press, Cambridge, UK, 1995).
[26] M. C. Jullien, J. Paret, and P. Tabeling, "Richardson pair dispersion in two-dimensional turbulence," Phys. Rev. Lett. **82**, 2872 (1999).
[27] V. Artale, G. Boffetta, A. Celani, M. Cencini, and A. Vulpiani, "Dispersion of passive tracers in closed basins: Beyond the diffusion coefficient," Phys. Fluids **9**, 3162 (1997).
[28] G. Boffetta and I. M. Sokolov, "Statistics of two-particle dispersion in two-dimensional turbulence," Phys. Fluids **14**, 3224 (2002).
[29] G. Gioia, G. Lacorata, E. P. Marques Filho, A. Mazzino, and U. Rizza, "Richardson's law in large-eddy simulations of boundary-layer flows," Boundary-Layer Meteorol. **113**, 187 (2004).
[30] G. Boffetta, A. Celani, A. Crisanti, and A. Vulpiani, "Pair dispersion in synthetic fully developed turbulence," Phys. Rev. E **60**, 6734 (1999).
[31] Z. S. She and E. Lévêque, "Universal scaling laws in fully developed turbulence," Phys. Rev. Lett. **72**, 336 (1994).
[32] E. Aurell, G. Boffetta, A. Crisanti, G. Paladin, and A. Vulpiani, "Predictability in the large: An extension of the concept of Lyapunov exponent," J. Phys. A **30**, 1 (1997).
[33] S. S. Girimaji and S. B. Pope, "Material element deformation in isotropic turbulence," J. Fluid Mech. **220**, 427 (1990).
[34] K. R. Sreenivasan and R. A. Antonia, "The phenomenology of small-scale turbulence," Annu. Rev. Fluid Mech. **29**, 435 (1997).